POLITECNICO DI TORINO
Repository ISTITUZIONALE

A Coplanar Waveguide Resonator Technique for the Characterization of Iron-Based Superconductors

Original
A Coplanar Waveguide Resonator Technique for the Characterization of Iron-Based Superconductors / Torsello, D., Ghigo, G.. - ELETTRONICO. - (2020), pp. 726-731. (2020 IEEE Ukrainian Microwave Week (UkrMW)) [10.1109/UkrMW49653.2020.9252603].

Availability:
This version is available at: 11583/2875960 since: 2021-03-24T17:00:13Z

Publisher:
Institute of Electrical and Electronics Engineers Inc.

Published
DOI:10.1109/UkrMW49653.2020.9252603

Terms of use:

This article is made available under terms and conditions as specified in the corresponding bibliographic description in the repository

Publisher copyright
IEEE postprint/Author's Accepted Manuscript

©2020 IEEE. Personal use of this material is permitted. Permission from IEEE must be obtained for all other uses, in any current or future media, including reprinting/republishing this material for advertising or promotional purposes, creating new collecting works, for resale or lists, or reuse of any copyrighted component of this work in other works.

(Article begins on next page)

26 November 2026

A coplanar waveguide resonator technique for the characterization of iron-based superconductors

Daniele Torsello
Politecnico di Torino, Dpt. Applied Science and Technology
Istituto Nazionale di Fisica Nucleare, Sezione di Torino
Torino, Italy
daniele.torsello@polito.it

Gianluca Ghigo
Politecnico di Torino, Dpt. Applied Science and Technology
Istituto Nazionale di Fisica Nucleare, Sezione di Torino
Torino, Italy
gianluca.ghigo@polito.it

***Abstract*—We present in detail a coplanar waveguide resonator (CPWR) method for the characterization of superconducting single crystals. It exploits the region of a CPWR where the rf magnetic field is quite homogeneous, by coupling a sample to it. Measurements are performed with and without the crystal, allowing a cavity perturbation approach. From the modifications in the resonance frequency and quality factor of the system it is possible to extract the London penetration depth and its anisotropy, quasiparticle conductivity, surface impedance and, when a coexisting magnetic phase is present, even bulk complex susceptibility.**

***Index Terms*—Microwave superconductivity, coplanar waveguide resonator, iron based superconductors, penetration depth, surface impedance**

I. Introduction

The response of superconductors in the presence of high frequency fields is particularly interesting both for applications and for fundamental studies. The discovery of high temperature superconductors (HTS) that can be employed for several devices such as filters [1] and, more recently, the employment of superconducting resonators in the realization and control of qubits [2] has been the driving force to engineer and optimize materials for high frequency applications.

From the point of view of materials investigation, high frequency techniques have provided access to several interesting quantities such as the London penetration depth, surface impedance, complex conductivity, scattering time and superfluid density [3], and the use of HTS resonators allows achieving high sensitivity [4]. This kind of studies yielded valuable insight in the coupling mechanism and gap structure of novel superconductors as the recently discovered iron pnictides [5]. In this context, we developed and optimized an experimental technique that gives access to the London penetration depth, superfluid density, quasiparticle conductivity and surface impedance of small samples of superconducting materials with a critical temperature T_c between $\simeq$ 10 and 50 K, such as the Iron based superconductors (IBSs). This technique makes use of a coplanar waveguide resonator (CPWR) made of a high temperature superconductor thin film and has been employed for extensive studies on the iron pnictides.

In this manuscript, the experimental technique is discussed at length in section II and some examples of its use and results are reported in section III, finally conclusions are drown (section IV).

This work was partially supported by the Italian Ministry of Education, University and Research (Project PRIN HIBiSCUS, Grant No. 201785KWLE) and by the Istituto Nazionale di Fisica Nucleare (CN5 - TERA experiment).

II. The CPWR technique

A. Experimental setup

The experimental setup currently employed in our laboratory for the CPWR technique consists of:

- a Cryomech PT-415 pulse-tube cooler, mechanically decoupled from the measurement area, that allows to obtain a base temperature at the sample position of about 5 K (limited mainly by the heat carried in by the coaxial cables),
- an Oxford temperature controller ITC503 equipped with a Cernox thermometer and two heaters that allow us to measure and control the temperature near the sample position with a 0.001 K sensibility,
- a Rohde Schwarz ZVK vector-network-analyzer that can operate up to 40 GHz,
- the measurement cell (schematized in panel (a) of Fig. 1) that consists of a CPWR obtained from a $YBa_2Cu_3O_{7-x}$ (YBCO) film with thickness t=250 nm on a non-magnetic MgO substrate. The resonator was patterned by standard optical litography on a commercial THEVA GmbH [6] film with T_c = 88 K [7]. The geometry is optimized to match the impedance (50 Ω) of the measuring system and to have a resonance frequency of about 8 GHz: the central strip is w=350 μm wide, about 8 mm long, and each ground plane is distant 150 μm from it. It should be noted that different resonance frequencies could be achieved by changing the length L of the central strip, since $f_0 \propto 1/L$. The YBCO film is positioned into a brass closed structure equipped with RF launchers.

The measurement cell is mounted on a long stand so that, if needed, it can be inserted in the bore of a magnet to perform

measurement with external DC magnetic field applied.

This setup allows to investigate materials in the shape

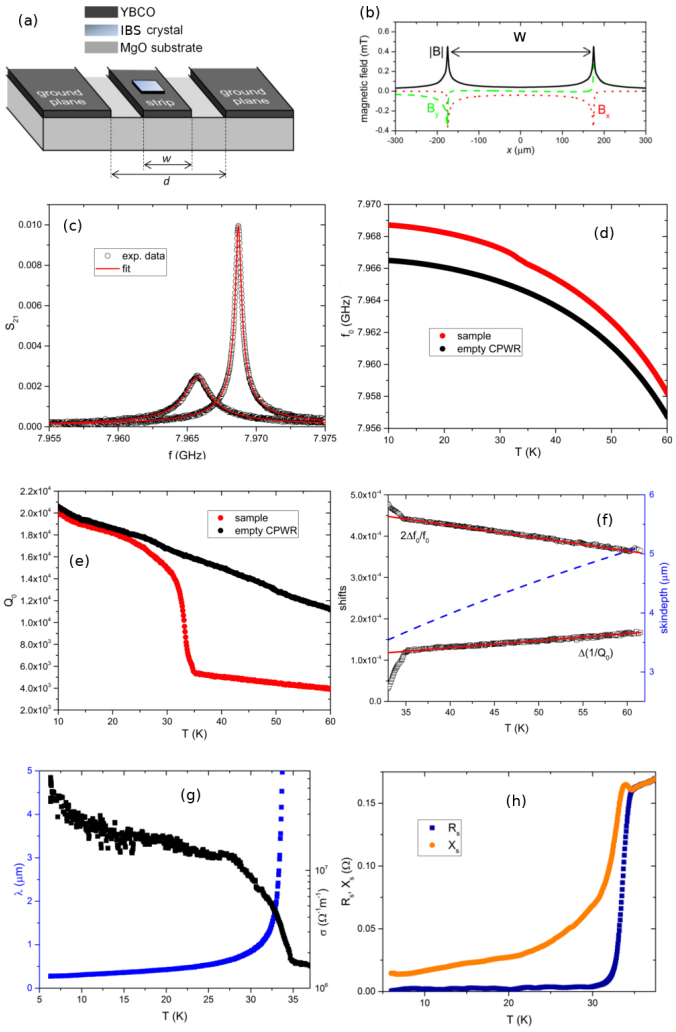


Fig. 1. Survey of the microwave characterization technique employed on a $CaKFe_4As_4$ single crystal. (a) Schematic illustration of the CPWR with the IBS sample coupled to it. (b) Rf magnetic field distribution near the sample position. (c) Frequency dependence of the transmission coefficient of the resonator with the sample coupled to it below and above the critical temperature of the material. Red curves are the fit described in the text. (d) Temperature dependence of the resonant frequency and (e) quality factor of the resonator by itself (black symbols) and of the resonator with the sample coupled to it (red symbols). (f) Resonance frequency and quality factor relative shifts above T_c and their fits by means of Eqs. 6 (red solid lines), as discussed in the text. The skin depth employed in the fits is shown as a blue dashed line. (g) Typical outcome of the measurements performed with the CPWR technique: $\lambda_L(T)$ (blue, left scale) and $\sigma_n(T)$ (black, right scale). (h) Surface impedance calculated with Eq. 12 from the data showed in (g).

of small platelets with typical dimensions $2a \times 2b \times 2c = 200 \times 350 \times 10\ \mu\text{m}^3$. The only constraint is $2a < w$ to avoid inhomogeneities in the field experienced by the sample.

The sample is coupled to the CPWR by placing it at the center of the waveguide strip with a small amount of vacuum grease that ensures adhesion and thermal contact. At this position, the electric field generated by the resonator is negligible (in fact, it is concentrated in the regions between the edges of the central strip and the edges of the ground planes) and the magnetic field has a maximum. Moreover, far from the strip edges, the magnetic field is uniform within 5% and the only nonzero component is the one parallel to the film surface, and in particular to w (in the ab-crystallographic plane of the sample). The field was evaluated (panel (b) of Fig. 1) using the Biot-Savart law on the current density distribution $j^{rf}(x)$ for the center conductor of a CPWR given by [8]:

$$j^{rf}(x) = \frac{I_{tot}}{K(\frac{w}{d})w\sqrt{\zeta(x)}} \tag{1}$$

where x is the coordinate along the transverse direction, I_{tot} is the total current,

$$\zeta(x) = \begin{cases} \frac{\lambda_{eff}}{w}\left[1-\left(\frac{w}{d}\right)^2\right], & 0 \le \frac{w}{2} - |x| < \lambda_{eff} \\ \left[1-\left(\frac{2x}{w}\right)^2\right]\left[1-\left(\frac{2x}{d}\right)^2\right], & |x| < \frac{w}{2} - \lambda_{eff} \end{cases} \tag{2}$$

K is the complete elliptic integral and the effective penetration depth of the YBCO thin film is $\lambda_{eff} = \lambda_L \coth(t/2\lambda_L)$. The resulting rf magnetic field produced at the sample position is the probe for the superconducting properties of the material. The resonator is operated below its nonlinearity threshold [9]. A continuous measurement of the transmission coefficient S_{21} in a frequency window around the CPWR resonance is performed while the system is heated from the base temperature to about 20-30K above the T_c of the sample. The typical heating rate is 0.25K/min, slow enough to ensure that no thermal drift effects influence the resonance curves. As shown in Fig. 1 (c), each $S_{21}(T)$ curve is fitted with a modified Lorentzian function $(S_{21}(f)=S_{21}^{max}/\sqrt{1+Q_L^2\,(f/f_0 - f_0/f)^2})$ superimposed to a linear background to yield the resonance frequency, f_0 and loaded quality factor Q_L of the system at a particular temperature. The unloaded quality factor, Q_0, is then calculated as $Q_0 = Q_L/(1-S_{21}^{max})$. In the end the $f_0(T)$ and $Q_0(T)$ curves are obtained. Two measurements are performed: one with and one without the samples, an example is shown in Fig. 1 (d) and (e). The relative shifts $\Delta f_0/f_0$ and $\Delta(1/Q_0)$ are then computed in order to analyze the properties of the sample with a cavity perturbation approach.

B. Data analysis

When, as in our case, a sample much smaller than the cavity is positioned in a region where $\boldsymbol{E}$ has a node and the fields outside the sample are not significantly influenced by its presence, it is possible to express the relative shifts as [10]:

$$\left(\frac{f-f_0}{f}\right) + j\left(\frac{1}{2Q} - \frac{1}{2Q_0}\right) \approx -\frac{\int_{V_S}(\mu-\mu_0)\,|\boldsymbol{H}_0|^2\,dV}{2\int_{V_C}\mu_0|\boldsymbol{H}_0|^2\,dV} \approx -\frac{1}{2}\Gamma\chi \tag{3}$$

where Γ takes into account all the geometrical factors connected to the distribution of the fields in the cavity and χ

is the complex magnetic susceptibility of the sample. In this approach, approximations act differently for quality factor and frequancy shifts, therefore two distinct geometrical factors (Γ and Γ') should be considered [10]. For a large slab of superconductor with non negligible losses, χ can be related to the complex propagation constant κ of the rf electromagnetic wave (which in turn, below T_c, is related to λ_L) yielding:

$$2\frac{\Delta f_0}{f_0} = \Gamma\left\{1 - \Re\left[\frac{\tanh\kappa c}{\kappa c}\right]\right\}, \tag{4}$$

$$\Delta\left(\frac{1}{Q_0}\right) = \Gamma'\Im\left[\frac{\tanh\kappa c}{\kappa c}\right]. \tag{5}$$

This last relation can also be modified to include a bulk magnetic contribution in the case of materials for which superconductivity and strong magnetic signals coexist [11].

The geometrical constants Γ and Γ' need to be determined self-consistently within a calibration procedure that makes use of the experimental data measured above T_c, where IBSs are metallic. For a metal $\Re(k) = \Im(k) = 1/\delta$, where $\delta = \sqrt{2\rho/(\omega\mu_0)}$ is the classical skin depth, related to the resistivity ρ. Moreover, due to the small size of the investigated samples that can not be considered infinite in any dimension, field penetration from all sides of the metallic sample should be considered due to demagnetization effects. Therefore, instead of only the term $(\tanh kc)/kc$ in Eqs. 4 and 5, we consider a sum over all three dimensions (x_i in the following equations runs on a, b and c) of analogous terms. In addition, by noticing that $\tanh z = (\sinh 2x + i\sin 2y)/(\cosh 2x + \cos 2y)$, where $z = x + iy$, one can rewrite Eqs. 4 and 5 as:

$$2\frac{\Delta f_0}{f_0} = \Gamma\left\{1 - \sum_1^3 A(x_i)\right\} \quad \Delta\left(\frac{1}{Q_0}\right) = \Gamma'\sum_1^3 B(x_i), \tag{6}$$

where

$$A(x_i) = \frac{\delta}{2x_i}\frac{sinh(2x_i/\delta) + sin(2x_i/\delta)}{cosh(2x_i/\delta) + cos(2x_i/\delta)} \tag{7}$$

$$B(x_i) = \frac{\delta}{2x_i}\frac{sinh(2x_i/\delta) - sin(2x_i/\delta)}{cosh(2x_i/\delta) + cos(2x_i/\delta)}. \tag{8}$$

This allows one to fit the experimental $\Delta f_0/f_0$ and $\Delta(1/Q_0)$ data above T_c (see Fig. 1 (f))) fixing the geometrical factors Γ and Γ'. It should be noted that both temperature dependences of $\Delta f_0/f_0$ and $\Delta(1/Q_0)$ are mainly due to the temperature dependence of the resistivity.

Once Γ and Γ' are fixed, Eqs. 4 and 5 can be inverted to yield the real and imaginary part of the propagation constant $\kappa = \alpha + i\beta$ over the whole measured temperature range. Then it is possible to calculate the London penetration depth λ_L and quasiparticle conductivity σ_n [12]:

$$\kappa = \alpha + i\beta = \sqrt{1/\lambda_L^2 + i\omega\mu_0\sigma_n} \tag{9}$$

Specifically, Eq. 9 can be rewritten as:

$$\sqrt[4]{1/\lambda_L^4 + \omega^2\mu_0^2\sigma_n^2}\cos\left(\frac{\arctan(\omega\mu_0\sigma_n\lambda_L^2)}{2}\right) = \alpha \tag{10}$$

$$\sqrt[4]{1/\lambda_L^4 + \omega^2\mu_0^2\sigma_n^2}\sin\left(\frac{\arctan(\omega\mu_0\sigma_n\lambda_L^2)}{2}\right) = \beta \tag{11}$$

that are solved numerically to yield λ_L and σ_n. Moreover these two quantities are connected with the surface impedance of the sample Z_s by [8]

$$Z_s = R_s + iX_s = \frac{i\omega\mu_0\lambda_L}{\sqrt{1 + i\omega\mu_0\sigma_n\lambda_L^2}}. \tag{12}$$

Therefore one can use them to calculate the surface resistance R_s and reactance X_s. Typical results of the measurement are shown in Fig. 1 (g) and (h) for the case of a $CaKFe_4As_4$ single crystal.

C. Uncertainties

In this section, the uncertainty on the main measured property (λ_L) is evaluated. This depends on:

- uncertainty in the determination of f_0 and Q_0 by Lorentzian fitting
- noise in the S_{21} measurement
- uncertainty in the determination of the temperature during the frequency scan
- possible small differences in the CPWR properties due to heating and cooling
- uncertainty in the determination of the crystal thickness
- uncertainty in the calibration (determination of the geometrical factors)

The first four sources affect the value of $\Delta f/f$ and $\Delta(1/Q)$, whereas the last two the value of Γ and Γ' in equations 4 and 5. Both then propagate to affect λ_L through the real and imaginary part of $\tanh(kc)/kc$. Let us now discuss them one by one for the typical measurement.

The Lorentzian fits are extremely reliable, with each fit yielding a reduced chi-squared $\tilde{\chi}^2 \lesssim 1$, resulting in an uncertain on the extracted values that is negligible if compared to other sources.

The noise of the measurement can be estimated by the spread of experimental data taken at the same temperature, and results in a (negligible) relative variation of $2{\cdot}10^{-6}\%$ for f_0 and 0.05% for Q_0 as shown in Fig. 2 (a)-(c).

The uncertainty on the temperature measurement (mainly due to the time needed for the frequency scan) can be considered to be $\pm$ 0.01K. No variations of the $f_0(T)$ and $Q_0(T)$ curves were observed with measurements carried out in heating and cooling mode with the same rate, as well as measurements carried out with lower heating rates.

In order to perform the reference measurement without the sample, the system is heated to room temperature and subsequently cooled again. This might produce slight changes in the CPWR properties (Fig. 2 (d)) that, however, have a minor impact on the final data. The maximum spread of $\Delta(1/Q)$ values is smaller than 10% and that of $\Delta f/f$

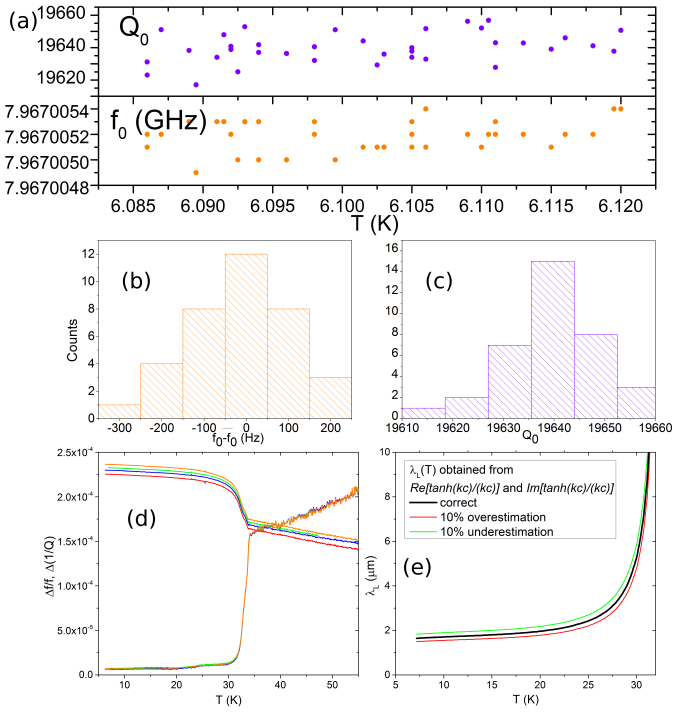


Fig. 2. Measurement (a) and distribution of the f_0 (b) and Q_0 (c) values of the empty resonator taken at 6.10K $\pm$ 0.02 K. The relative variation is $2{\cdot}10^{-6}\%$ for f_0 and 0.05% for Q_0. $\overline{f_0}$ is the average value of f_0. (d) $\Delta f/f$ and $\Delta(1/Q)$ curves obtaind by repeated measurements (several days apart) of the empty resonator that has been brought to room temperature between each measurement. (e) Modifications of $\lambda_L(T)$ produced by a 10% overestimation and underestimation of the real and imaginary part of $\tanh(kc)/kc$.

is smaller than 5% for measurements performed several days apart and for which the system experienced a large number of heating and cooling cycles, whereas the real reference measurement is always done directly after the measurement with the sample. Moreover, these modifications are close to a rigid shift and can be effectively accounted for during the determination of the geometrical factors in the calibration procedure, yielding a rather small influence on the absolute valute of λ_L, and not affecting at all its temperature dependence.

The sample thickness is determined employing an optical microscope and is accompanied by an uncertainty of about 0.5 μm, that can be the major source of uncertainty in the case of particularly thin samples since it directly affects the determination of the penetration depth (at low temperature $\lambda_L \simeq c \cdot [(\Delta 1/Q)^2 + (2\Delta f/f - \Gamma)^2]/[\Gamma(\Gamma - 2\Delta f/f]$).

Finally, the uncertainty related to the calibration procedure itself (and therefore on the geometrical factors) is usually negligible due to the strong constraints given by the temperature dependece of both $\Delta f/f$ and $\Delta(1/Q)$ (as visible in Fig. 1 (f)).

As stated in the beginning of this section, all the above mentioned sources of uncertainty affect the real and imaginary part of $\tanh(kc)/kc$. The propagation of all these uncertainty contributions is almost straightforward: a $\pm$ 10% uncertainty in the determination of the real and imaginary part of $\tanh(kc)/kc$ (independently on the source) propagates to produce an uncertainty in the determination of λ_L absolute value of +11%/-9%, whereas the temperature dependence of λ_L is affected in a negligible way (see Fig. 2 (e)). In the end, by adding up all the above discussed contributions and considering the way they propagate down to the determination of the London penetration depth, we generally obtain an uncertainty on λ_L between 5% and 10%.

III. Case studies

The CPWR technique presented in detail in the previous section has been employed to investigate several IBSs. Here a selection of results is presented in order to show the possibile studies that can be carried out.

A. Anisotropic properties

We have recently shown that the CPWR technique allows one to study the London penetration depth anisotropy through the measurement of samples with different aspect ratios. In fact, most IBSs show a layered structure, yielding to different values of in-plane λ_{ab} and out-of-plane λ_c. The penetration depth anisotropy $\gamma_L = \lambda_c/\lambda_{ab}$ is relevant for application of superconducting materials such as the production of coated conductors for high magnetic field applications, since it represents the intrinsic anisotropy of the material without the effect of vortex pinning [13]. Moreover, other techniques allow only the measurement of the in-plane component of the penetration depth, therefore it is useful to obtain this quantity to compare results obtained with different approaches.

B. Technique comparison

In order to validate the technique, a comparative study on $CaKFe_4As_4$ has been carried out [14] between the CPWR, the tunnel diode resonator (TDR) [15] and the NV centers in diamond magnetometry techniques [16]. As visible from Fig. 3, a full characterization of the London penetration depth was achieved with a remarkable agreement between the data obtained with the three techniques as well as with literature data from μSR experiments [17].

C. Materials characterization

The study of $\lambda_L(T)$ and $\sigma_n(T)$, especially if supported by theoretical calculations, can be very effective in the investigation of the fundamental properties of superconductors and their relation to different structural properties. In this regard, a study was carried out [18] on the $BaFe_2As_2$ (Ba-122) family covering all possible typologies of substitution to induce superconductivity: K for Ba, Co for Fe and P for As. Through the analysis of the experimental data within a three component Eliashberg model based on coupling provided by antiferromagnetic spin fluctuations, it has been possible to confirm the symmetry of the order parameter in these systems as $s_\pm$ without line nodes in the gap and to highlight the role

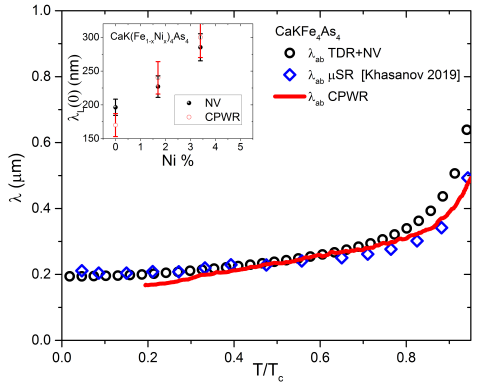


Fig. 3. Comparison of the λ_L measurement results from different technique on the same material ($CaK(Fe,Ni)_4As_4$). TDR and NV data from [14], μSR data from [17].

of substitution within the superconducting FeAs planes in the determination of the superconducting properties. A selection of results for the different compounds is summarized in table I.

TABLE I

SUMMARY OF THE PROPERTIES CHARACTERIZED BY THE COMBINATION OF EXPERIMENTAL DATA AND THEORETICAL MODEL FOR THE THREE DIFFERENT DOPANTS OF THE BA-122 FAMILY. T_c IS THE EXPERIMENTAL CRITICAL TEMPERATURE, $\lambda_L^{exp}(0)$ IS THE LOW-TEMPERATURE PENETRATION DEPTH, $\sigma(T_c)$ IS THE MICROWAVE CONDUCTIVITY AT T_c, AND $\Delta_i^R(0)$ ARE THE LOW-TEMPERATURE VALUES OF THE GAPS.

dopant	T_c (K)	$\lambda_L^{exp}(0)$ (nm)	$\sigma(T_c)$ ($\Omega^{-1}m^{-1}$)	$\Delta_1^R(0)$ (meV)	$\Delta_2^R(0)$ (meV)	$\Delta_3^R(0)$ (meV)
K	38.7	197	$1.95{\cdot}10^6$	12.0	5.4	-12.0
Co	24.2	165	$0.47{\cdot}10^6$	7.2	-3.9	-7.8
P	29.0	160	$1.13{\cdot}10^6$	3.8	10.8	-8.3

D. Effects of disorder

The fact that the CPWR technique is completely non-destructive on the investigated samples makes it ideal for investigating the effects of disorder on the superconducting properties. Disorder can be introduced by ion irradiation in different forms depending on the nature and energy of the chosen ion: columnar, correlated and point-like defects. The fact that samples are not damaged by the experimental technique is pivotal for repeated irradiation experiments needed to achieve high total doses and to investigate step by step the dependency on the amount of disorder. This approach allowed us, also with the support of Eliashberg calculations, to show that the weak rate of suppression of T_c with disorder is not in disagreement with the $s_\pm$ symmetry of the order parameter and with the observed strong modifications to λ_L [19]. Moreover, it has been possible to experimentally observe the theoretically predicted [20] transition from the $s_\pm$ to the s_{++} order parameter driven by disorder [21] (see Fig. 4). The fact that the CPWR technique also gives access to σ_n and Z_s also proved valuable to identify novel signatures of this transition [22], [23].

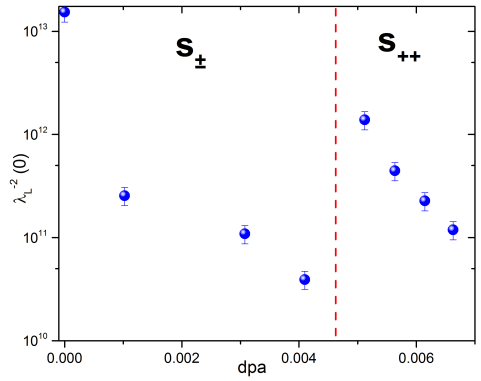


Fig. 4. Experimental observation of the theoretically predicted increase of the superfluid density at the $s_\pm$ to s_{++} disorder-driven transition. The amount of disorder in the sample is expressed in terms of displacement per atom (dpa) as estimated by Monte Carlo codes PHITS [24] and SRIM [25].

IV. CONCLUSIONS

In summary, the CPWR technique is a powerful tool to investigate the properties of superconducting materials with intermediate T_c. It allows a complete characterization of the critical temperature, London penetration depth, superfluid density, quasiparticle conductivity and surface impedance. The uncertainty of the measurement affects mostly the absolute value of λ_L and in a typical case is smaller than 10%. Such a large set of information can be combined to theoretical models yielding a deeper understanding of the mechanism of superconductivity in novel materials. Moreover, the technique does not damage the sample and is therefore particularly suitable for investigating the effect of disorder on the superconducting properties.

ACKNOWLEDGMENT

The authors thank R. Prozorov, M. A. Tanatar, P. C. Canfield and T. Tamegai for providing the samples; and L. Gozzelino, R. Gerbaldo and F. Laviano for fruitful discussion and for their contribution in the irradiation experiments.

REFERENCES

[1] B. H. Moeckly and Y. Zhang, "Strontium titanate thin films for tunable $YBa_2Cu_3O_7$ microwave filters," *IEEE Transactions on Applied Superconductivity*, vol. 11, no. 1, pp. 450–453, March 2001.

[2] L. Frunzio, A. Wallraff, D. Schuster, J. Majer, and R. Schoelkopf, "Fabrication and characterization of superconducting circuit qed devices for quantum computation," *IEEE Transactions on Applied Superconductivity*, vol. 15, no. 2, pp. 860–863, June 2005.

[3] G. Ghigo, D. Torsello, R. Gerbaldo, L. Gozzelino, F. Laviano, and T. Tamegai, "Effects of heavy-ion irradiation on the microwave surface impedance of $(Ba_{1-x}K_x)Fe_2As_2$ single crystals," *Superconductor Science and Technology*, vol. 31, no. 3, p. 034006, feb 2018.

[4] A. Barannik, N. T. Cherpak, M. A. Tanatar, S. Vitusevich, V. Skresanov, P. C. Canfield, and R. Prozorov, "Millimiter-wave surface impedance of optimally-doped $Ba(Fe_{1-x}Co_x)_2As_2$ single crystals," *Phys. Rev. B*, vol. 87, p. 014506, Jan 2013.

[5] G. Ghigo, G. A. Ummarino, L. Gozzelino, and T. Tamegai, "Penetration depth of $(Ba_{1-x}K_x)Fe_2As_2$ single crystals explained within a multiband eliashberg $s_\pm$ approach," *Phys. Rev. B*, vol. 96, p. 014501, Jul 2017.

[6] Https://www.theva.com.

[7] G. Ghigo, F. Laviano, R. Gerbaldo, and L. Gozzelino, "Tuning the response of YBCO microwave resonators by heavy-ion patterned micro-channels," *Superconductor Science and Technology*, vol. 25, no. 11, p. 115007, sep 2012.

[8] I. Vendik, *High temperature superconductor devices for microwave signal processing - Part II*. St. Petersburg: Skladen Co, 1997.

[9] G. Ghigo, R. Gerbaldo, L. Gozzelino, F. Laviano, and T. Tamegai, "Penetration depth and quasiparticle conductivity of Co- and K-doped $BaFe_2As_2$ crystals, investigated by a microwave coplanar resonator technique," *IEEE Transactions on Applied Superconductivity*, vol. 26, no. 3, pp. 1–4, April 2016.

[10] L.-F. Chen, C. Ong, C. Neo, V. Varadan, and V. K. Varadan, *Microwave electronics: measurement and materials characterization*. John Wiley & Sons, 2004.

[11] G. Ghigo, D. Torsello, L. Gozzelino, T. Tamegai, I. S. Veshchunov, S. Pyon, W. Jiao, G.-H. Cao, S. Y. Grebenchuk, I. A. Golovchanskiy, V. S. Stolyarov, and D. Roditchev, "Microwave analysis of the interplay between magnetism and superconductivity in $EuFe_2(As_{1-x}P_x)_2$ single crystals," *Phys. Rev. Research*, vol. 1, p. 033110, Nov 2019.

[12] I. Vendik, "Phenomenological model of the microwave surface impedance of high-tcsuperconducting films," *Superconductor Science and Technology*, vol. 13, no. 7, pp. 974–982, jun 2000.

[13] D. Torsello, G. A. Ummarino, J. Bekaert, L. Gozzelino, R. Gerbaldo, M. A. Tanatar, P. C. Canfield, R. Prozorov, and G. Ghigo, "Tuning the Intrinsic Anisotropy with Disorder in the $CaKFe_4As_4$ Superconductor," *Phys. Rev. Appl.*, vol. 13, p. 064046, Jun 2020.

[14] D. Torsello, K. Cho, K. R. Joshi, S. Ghimire, G. A. Ummarino, N. M. Nusran, M. A. Tanatar, W. R. Meier, M. Xu, S. L. Bud'ko, P. C. Canfield, G. Ghigo, and R. Prozorov, "Analysis of the london penetration depth in ni-doped $CaKFe_4As_4$," *Phys. Rev. B*, vol. 100, p. 094513, Sep 2019.

[15] R. Prozorov and V. G. Kogan, "London penetration depth in iron-based superconductors," *Reports on Progress in Physics*, vol. 74, no. 12, p. 124505, sep 2011.

[16] K. Joshi, N. Nusran, M. Tanatar, K. Cho, W. Meier, S. Bud'ko, P. Canfield, and R. Prozorov, "Measuring the lower critical field of superconductors using nitrogen-vacancy centers in diamond optical magnetometry," *Phys. Rev. Applied*, vol. 11, p. 014035, Jan 2019.

[17] R. Khasanov, W. R. Meier, S. L. Bud'ko, H. Luetkens, P. C. Canfield, and A. Amato, "Anisotropy induced vortex lattice rearrangement in $CaKFe_4As_4$," *Phys. Rev. B*, vol. 99, p. 140507, Apr 2019.

[18] D. Torsello, G. A. Ummarino, L. Gozzelino, T. Tamegai, and G. Ghigo, "Comprehensive eliashberg analysis of microwave conductivity and penetration depth of K-, Co-, and P-substituted $BaFe_2As_2$," *Phys. Rev. B*, vol. 99, p. 134518, Apr 2019.

[19] G. Ghigo, G. Ummarino, L. Gozzelino, R. Gerbaldo, F. Laviano, D. Torsello, and T. Tamegai, "Effects of disorder induced by heavy-ion irradiation on $(Ba_{1-x}K_x)Fe_2As_2$ single crystals, within the three-band eliashberg $s_\pm$wave model," *Scientific reports*, vol. 7, no. 1, p. 13029, 2017.

[20] D. V. Efremov, M. M. Korshunov, O. V. Dolgov, A. A. Golubov, and P. J. Hirschfeld, "Disorder-induced transition between $s_\pm$ and s_{++} states in two-band superconductors," *Phys. Rev. B*, vol. 84, p. 180512, Nov 2011.

[21] G. Ghigo, D. Torsello, G. A. Ummarino, L. Gozzelino, M. A. Tanatar, R. Prozorov, and P. C. Canfield, "Disorder-driven transition from $s_\pm$ to s_{++} superconducting order parameter in proton irradiated $Ba(Fe_{1-x}Rh_x)_2As_2$ single crystals," *Phys. Rev. Lett.*, vol. 121, p. 107001, Sep 2018.

[22] D. Torsello, R. Gerbaldo, L. Gozzelino, M. A. Tanatar, R. Prozorov, P. C. Canfield, and G. Ghigo, "Electrodynamic response of $Ba(Fe_{1-x}Rh_x)_2As_2$ across the $s_\pm$to s_{++} order parameter transition," *The European Physical Journal Special Topics*, vol. 228, no. 3, pp. 719–723, 2019.

[23] D. Torsello, G. A. Ummarino, R. Gerbaldo, L. Gozzelino, and G. Ghigo, "Eliashberg analysis of the electrodynamic response of $Ba(Fe_{1-x}Rh_x)_2As_2$ across the $s_\pm$to s_{++} order parameter transition," *Journal of Superconductivity and Novel Magnetism*, pp. 1–6, 2019.

[24] T. Sato, K. Niita, N. Matsuda, S. Hashimoto, Y. Iwamoto, S. Noda, T. Ogawa, H. Iwase, H. Nakashima, T. Fukahori, K. Okumura, T. Kai, S. Chiba, T. Furuta, and L. Sihver, "Particle and heavy ion transport code system, phits, version 2.52," *Journal of Nuclear Science and Technology*, vol. 50, no. 9, pp. 913–923, 2013.

[25] J. F. Ziegler, M. D. Ziegler, and J. P. Biersack, "Srim–the stopping and range of ions in matter (2010)," *Nuclear Instruments and Methods in Physics Research Section B: Beam Interactions with Materials and Atoms*, vol. 268, no. 11-12, pp. 1818–1823, 2010.